ACS OMEGA

http://pubs.acs.org/journal/acsodf

Perspective

In Situ Spectroelectrochemical Investigations of Electrode-Confined Electron-Transferring Proteins and Redox Enzymes

Daniel H. Murgida*

Cite This: *ACS Omega* 2021, 6, 3435−3446

Read Online

ACCESS | Metrics & More | Article Recommendations

ABSTRACT: This perspective analyzes recent advances in the spectroelectrochemical investigation of redox proteins and enzymes immobilized on biocompatible or biomimetic electrode surfaces. Specifically, the article highlights new insights obtained by surface-enhanced resonance Raman (SERR), surface-enhanced infrared absorption (SEIRA), protein film infrared electrochemistry (PFIRE), polarization modulation infrared reflection−absorption spectroscopy (PMIRRAS), Förster resonance energy transfer (FRET), X-ray absorption spectroscopy (XAS), electron paramagnetic resonance (EPR), and differential electrochemical mass spectrometry (DMES)-based spectroelectrochemical methods on the structure, orientation, dynamics, and reaction mechanisms for a variety of immobilized species. This includes small heme and copper electron shuttling proteins, large respiratory complexes, hydrogenases, multicopper oxidases, alcohol dehydrogenases, endonucleases, NO-reductases, and dye decolorizing peroxidases, among other enzymes. Finally, I discuss the challenges and foreseeable future developments toward a better understanding of the functioning of these complex macromolecules and their exploitation in technological devices.

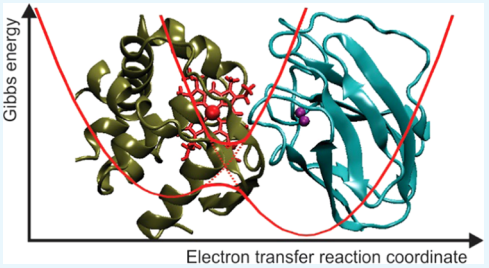

INTRODUCTION

Electron-transferring proteins and redox enzymes are key players in a large variety of metabolic processes, including photosynthetic and respiratory energy transductions. Their redox cofactors are quite diverse, including metallic centers and organic molecules that span a potential range of about 1.5 V.[1] The use of solution electrochemical and spectroelectrochemical methods, mainly with UV−vis and IR detection and with the aid of redox mediators, is a powerful approach for assessing thermodynamic redox parameters of these complex biomolecules, as well as for studying redox-linked structural changes.[2−4] Alternatively, redox proteins can be immobilized on the surface of electrodes following a variety of biocompatible or biomimetic approaches[5−9] to perform either mediated or direct electrochemistry. The latter approach circumvents protein diffusion and allows for some control on the protein−electrode distance and relative orientation, thus facilitating kinetic direct electron transfer (ET) studies by conventional electrochemical methods. This methodology and particularly the so-called protein film voltammetry technique have provided a great insight into the mechanistic aspects of several electron-transferring proteins and redox enzymes.[10] Moreover, it provides the basis for exploiting bioelectrocatalysis in enzymatic fuel cells, enzyme electrosynthesis, bio-photovoltaic devices, and biosensors.[6,11−14] However, conventional electrochemical techniques, such as voltammetry and chronoamperometry, provide limited information on the immobilized proteins. Coupling protein film electrochemistry with various types of spectroscopic detection allows us to obtain more detailed information on the structure, orientation, conformational dynamics, electronic properties, and chemical transformations associated with the ET and catalytic cycles of the immobilized redox proteins and enzymes.[3,9,15−18] In this perspective, I discuss selected examples of spectroelectrochemical studies of surface-confined redox proteins and enzymes, with focus on the contributions over the last 5 to 10 years. The spectroelectrochemical techniques employed in these selected examples include surface-enhanced resonance Raman (SERR) spectroscopy,[9,16] surface-enhanced infrared absorption (SEIRA),[7] protein film infrared electrochemistry (PFIRE),[19] polarization modulation infrared reflection−absorption spectroscopy (PMIRRAS),[20] electrochemical Förster resonance energy transfer (FRET),[21] in situ X-ray absorption spectroscopy (XAS),[22] in situ electron paramagnetic resonance (EPR),[23] and differential electrochemical mass spectrometry (DMES).[24] In all of the cases, proteins are either physisorbed or chemisorbed onto the working electrode (WE) surface, which is usually functionalized with different organic films that range from self-assembled monolayers (SAMs) of mercaptans on Au or Ag to more complex constructs that may include supported lipid

Received: November 25, 2020
Accepted: January 19, 2021
Published: January 27, 2021

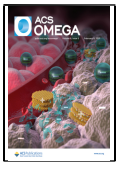

bilayers for biomimetic immobilization of membrane proteins.[5−9,16]

In the first part of the article, I introduce a recently developed theoretical framework for rationalizing the heterogeneous protein ET step, based on kinetic data collected using electrochemical and spectroelectrochemical methods. The second part provides an overview of lessons learned from spectroelectrochemical studies of 13 different types of proteins. The material is organized according to the proteins rather than by techniques as the aim is to exemplify the kind of information that can be obtained rather than introducing the technical aspects of each technique, which, however, can be found in the specific references provided in each case. This information crucially contributes to a better understanding of the functioning of these biomolecules and paves the way for their utilization in devices that rely upon protein immobilization.

ON THE HETEROGENEOUS ET STEP

Proteins are rather flexible macromolecules capable of exploring highly multidimensional and hierarchical free energy landscapes at physiological temperatures. Accordingly, kinetic and thermodynamic ET parameters of redox proteins are not only determined by crucial structural elements, such as the coordination sphere of a redox-active metal but also by protein flexibility and dynamics. For example, as discussed in subsequent sections, flexibility at different levels of the metalloprotein structure has been found to be a determinant for electron shuttling and alternative functions of multifunctional proteins such as cytochrome *c* (Cyt-c).[25] These dynamical features, particularly the low-frequency motions, are likely to be affected upon protein immobilization onto either electrodes or onto biological interfaces, as well as by the high viscosities typical of crowded media such as cells and organelles.[26] Therefore, while the Marcus semiclassical expression for long-range (nonadiabatic) ET reactions[27] is useful for most in vitro studies in diluted aqueous solutions, some of its underlying assumptions may not be fulfilled for proteins immobilized on electrodes or even under physiological conditions.[28] For example, water−protein nuclear fluctuations are assumed to be much faster than electron tunneling at the crossing point of reactant and product parabolas. This assumption may break down due to either slowdown of nuclear modes imposed by the medium or enhanced electron tunneling probability. So far, most theoretical and experimental efforts to address dynamical effects in ET have focused on ultrafast reactions.[29,30] For a slower ET process in the sub-millisecond timescale, direct electrochemistry and spectroelectrochemistry have proven useful tools for extracting thermodynamic and kinetic parameters, specifically for electron shuttling metalloproteins that contain the metal center partially exposed or very close to the surface. In recent years, different groups have investigated the heterogeneous ET reactions of a variety of native and non-native redox metalloproteins, including heme proteins such as cytochromes *c*, c_6, and b_{562}, as well as binuclear (Cu_A) and mononuclear (T1) copper proteins either physisorbed or chemisorbed on metal electrodes coated with SAMs of mercaptans with different compositions.[26,31−46] A common feature experimentally observed for all of these systems is a transition in the distance dependence of the zero driving force ET rate constants (k^0_{ET}) from an exponential decay at long protein−electrode distances to a plateau at shorter distances. Some examples are shown in Figure 1A,B. This type of behavior has been rationalized using a variety of arguments, depending on the experimental information available in each case. This includes a two-state conformational or orientational gating from a redox-inactive to a redox-active orientation of the adsorbed protein, as well as an electric-field controlled dynamical gating from populations with low electronic coupling to populations with higher electronic coupling.[40−43,47,48] In these models, the rate-limiting step at the thinner SAMs is reorientation rather than ET. On the other hand, it has been shown that in some cases the measured ET quantities reflect a distribution of orientations,[39] and that this distribution may be the origin of the unusual distance dependencies exemplified in Figure 1, even if protein orientations do not change during the experiment.[49]

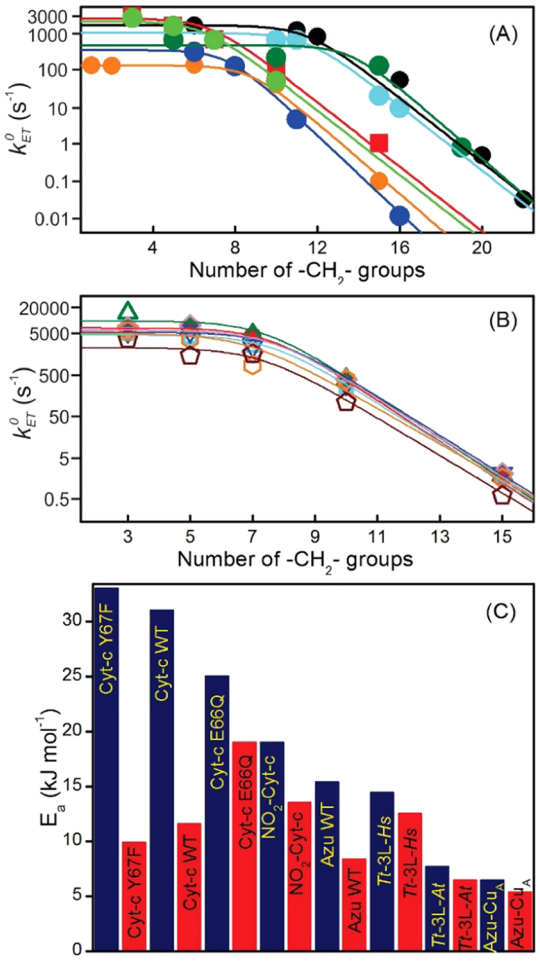

Figure 1. k^0_{ET} of heme (A) and copper (B) proteins immobilized on SAM-coated electrodes as a function of the chain lengths, as determined electrochemically or spectroelectrochemically. The lines are fittings to Matyushov's equations. Panel (A) includes Cyt-c wired to pyridinyl-terminated SAMs (black) adsorbed on COOH/OH (red) and COOH (orange) SAMs and cross-linked to COOH/OH-SAMs (light green), as well as Cyt-c_6 (light blue) and Cyt-D (green) on CH_3/OH-SAMs. Panel (B) includes azurin (Azu; red) and Cu_A (green) native proteins, as well as five chimeric proteins. Light blue, blue, and wine symbols correspond to the Cu_A scaffold that has been engineered to host the T1 copper sites of azurin (Azu-CuA), amicyanin (Ami-Cu_A), and the CBP protein (CBP-Cu_A), respectively. Pink and orange symbols are Cu_A chimeras containing the *Thermus thermophilus* scaffold and loops from other species (*Tt*-3L-*Hs* and *Tt*-1L-*E*, respectively). (C) ET activation energies of proteins adsorbed on thick (C_{15}-SAMs; blue) and thin (C_5-SAMs; red) coatings. The data correspond to WT Cyt-c, its point mutants Y67F and E66Q, Cyt-c nitrated at Tyr74 (NO_2-Cyt-c), WT Azu, and the chimeras Azu-Cu_A, *Tt*-3L-*Hs*, and *Tt*-3L-*At*. Figures are created using data taken from refs 26, 31, 32, 35, 36, 38, 39.

https://dx.doi.org/10.1021/acsomega.0c05746
ACS Omega 2021, 6, 3435−3446

Interestingly, ET activation energies of some adsorbed proteins, determined from either the temperature or overpotential dependencies of k_{ET}, were found to increase upon shortening the tunneling distances (Figure 1C),[26,31,32,34,37,50,51] in parallel with a change of sign of the activation volume.[37]

Waldeck and co-workers interpreted these findings, which are not consistent with a gating model, in terms of a change of the ET regime from nonadiabatic at the thicker SAMs to friction-controlled ET in the plateau region.[32,45,46] Albeit with some variability depending on the protein and immobilization method, the transition is generally observed at SAM thicknesses of about 10 methylene groups, which correspond to through-bond tunneling distances of ca. 19 Å (Figure 1A,B). For longer distances, i.e., in the nonadiabatic regime, the rate constant can be treated in terms of the Marcus semiclassical equation integrated to account for the density of states of the metal electrode, which can be approximated as

$$k_{NA} = \frac{\Delta}{\hbar}\mathrm{erfc}\left(\frac{\lambda + e\varphi}{\sqrt{4k_B T}}\right) \quad (1)$$

where $\Delta = \Delta_0 \exp(-\beta(R + R_0))$ is the protein−electrode coupling strength, which decays with the distance R at a rate $\beta \approx 1$ Å^{-1}. k_B is the Boltzmann constant, $\hbar$ is the reduced Planck constant, φ is the electrode overpotential with respect to the protein reduction potential ($E^{\circ\prime}$), erfc is the complementary error function, and λ is the effective ET reorganization energy, which differs from the Marcus definition for nonergodic systems.

For shorter electrode−protein distances, eq 1 is empirically corrected by a crossover parameter g to account for dynamical effects (friction control)[52]

$$k_{ET} = k_{NA}/(1 + g) \quad (2)$$

The limiting cases of nonadiabatic and friction−controlled ET reactions are obtained for $g \ll 1$ and $g \gg 1$, respectively. The latter has been ascribed to solvent dynamics affecting the crossing at the top of the activation barrier when the medium relaxation time exceeds the time of electron tunneling at the activated state. In this case, the crossover parameter for the electrochemical reaction of the surface-confined species is defined as[52]

$$g = 8\tau_x \Delta k_B T/\lambda\hbar \quad (3)$$

where the average Stokes-shift relaxation time τ_x represents the decay of the time-correlation function of the reaction coordinate. Note that the combination of eqs 1−3 leads to the experimentally observed distance dependence of k_{ET}^0 (Figure 1A,B), including the plateau and exponential regions. This agreement, however, is only apparent as the relaxation times required to enter the frictional control regime, i.e., $g \gg 1$, are about 200 ns, which is 6 orders of magnitude slower than the longitudinal relaxation time in bulk water and 3 orders slower than molecular dynamics (MD) simulation estimates of τ_x for protein/SAM/electrode systems.[53] This strong discrepancy reveals that low-frequency dynamical features need to be explicitly considered, in addition to fast nuclear medium modes. Waldeck et al.[32,45,46] addressed this issue using an adaptation of Zusman's equations. This approach leads to a reasonable qualitative description of the experiments, but relies upon approximations that are not fulfilled when reactants are attached to the electrode surface.[52]

Recently, Matyushov[52] introduced a novel phenomenological formalism where the distance of the immobilized protein to the electrode is described by overdamped oscillations of the protein in a soft harmonic potential with force constant κ, such that the average electronic coupling $\langle\Delta\rangle$ can be expressed as

$$\langle\Delta\rangle = \Delta \exp[3\beta^2 k_B T/2\kappa] \quad (4)$$

and the crossover parameter is

$$g = \tau_{eff}\langle\Delta\rangle/\hbar \quad (5)$$

The effective relaxation time τ_{eff} is a function of the characteristic times τ_x and τ_R, with $\tau_R = (\beta^2 D_R)^{-1}$ and D_R an effective diffusion coefficient that accounts for the oscillatory motions of the protein at the interface.

This theory has been recently contrasted with experimental results obtained for Cyt-c, azurin, and Cu_A centers.[50,52] The combination of eqs 1, 2 and 5, with Δ replaced by $\langle\Delta\rangle$, allowed for quantitative fitting of the observed distance dependencies of k_{ET}^0 in the entire range, yielding τ_{eff} and τ_R values in the microsecond and nanosecond timescales, respectively.[50,52] Consistently, τ_{eff} and τ_R values were found to be protein specific and to decrease with the flexibility of the scaffold and with the diffusion coefficient, respectively.[50] The data suggest that the amplitude of the oscillation is an effective parameter that represents a convolution of linear motion and angular reorientation coupled with interfacial water dynamics, in agreement with previous molecular dynamics simulations and time-resolved surface-enhanced resonance Raman investigations of Cyt-c on SAM-coated electrodes.[33,47,48,54]

The model predicts higher ET activation energies in the frictional control regime, E_a(FC), compared to the nonadiabatic regime, E_a (NA), in agreement with the experiments (Figure 1C)

$$E_a(\mathrm{NA}) = \frac{\lambda}{4} - \frac{(\beta k_B T)^2}{2\kappa} < E_a(\mathrm{FC}) = \frac{\lambda}{4} + \frac{(\beta k_B T)^2}{\kappa} + E_s \quad (6)$$

Moreover, incorporation of the experimentally verified power law dependencies of k_{ET}[26,31,32,37,50,51] and τ_{eff}[50] with medium viscosity (η) into the model, allows for the definition of the crossover parameter g in terms of protein-specific empirical parameters that reflect the sensitivity to η of relevant protein motions.[50]

An important outcome of these studies is that τ_x and τ_R have similar magnitudes, which results in frictional control even at electron tunneling distances as long as 19 Å. Moreover, the frictional control is strongly enhanced by the medium viscosity. These findings suggest that frictional control is likely to be an important feature in long-range intra- and intermolecular ET reactions in vivo, particularly in mitochondrial respiration as intramitochondrial viscosities vary between ca. 40 and 400 cP, depending on the physiological conditions. The sensitivity to the viscosity, and therefore the crossover parameter, is dictated by the specific dynamical features of each metalloprotein.

SPECTROELECTROCHEMICAL CASE STUDIES

Cytochrome *c* (Cyt−c). This small monohemic protein mediates ET from complex III to complex IV in the mitochondrial respiratory chains and has a number of alternative proapoptotic functions such as cardiolipin (CL) peroxidation, apoptosome assembly, and histone chaperone inhibition.[25,55] The heme iron of the native Cyt-c has a hexacoordinate low-spin

https://dx.doi.org/10.1021/acsomega.0c05746
ACS Omega 2021, 6, 3435−3446

(6cLS) configuration with Met80 and His18 as axial ligands (horse heart Cyt-c numbering; Figure 2A).

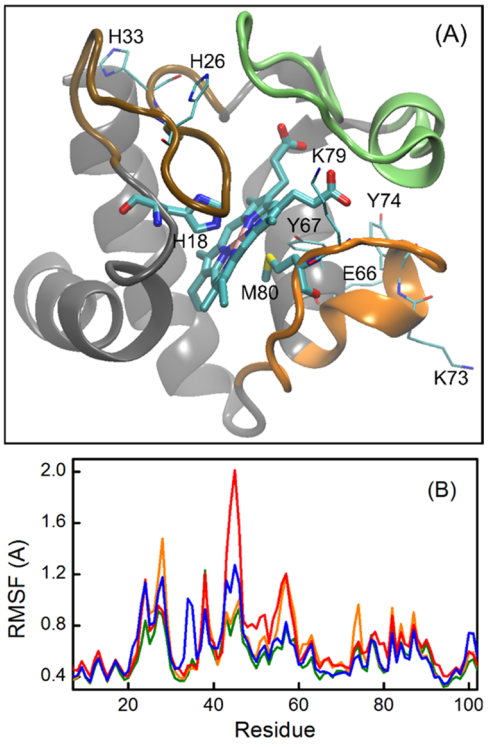

Figure 2. (A) Crystallographic structure of ferric horse heart Cyt-c (PDB 1HRC). Ω-loops 20−35, 40−57, and 70−85 are represented in ocher, lime, and orange, respectively. (B) Per residue root-mean-square fluctuations (RMSF) of different Cyt-c variants. Red: Y67F, blue: NO_2Cyt-c, orange: WT Cyt-c, and green: E66Q. Adapted with permission from ref 31. Copyright 2020, Elsevier.

Cyt-c has been the subject of an enormous amount of fundamental and applied research,[25] including a number of SERR and SEIRA spectroelectrochemical investigations starting with the seminal work by Hildebrandt and Stockburger in 1989.[56] Part of this work has been summarized in previous review articles.[9,16,17,57] In most (spectro)electrochemical studies, the protein is electrostatically adsorbed on SAM-coated electrodes containing carboxylate functional groups,[9,16,17,31,33,47,58−63] although adsorption,[36,64−67] cross-linking,[54] and wiring[32] to other types of SAMs have also been reported. SERR and SEIRA experiments, in combination with molecular dynamics simulations, show that adsorption of Cyt-c to negatively charged SAMs involves the patch of positively charged lysine residues that surround the partially exposed heme edge and that constitutes the binding site to natural partner biomolecules.[33,36,48,65,68] Increasing electric fields at the SAM/protein interface have been shown to induce conformational transitions of the adsorbed Cyt-c that do not necessarily involve significant alteration of the secondary structure but a motion of the flexible Ω-loops (Figure 2A), which in turn leads to the detachment of the labile sixth ligand Met80, particularly in the ferric state. This axial position may either remain vacant, leading to a five-coordinate high spin (5cHS) heme or be occupied by two alternative His residues (His33 or His26) leading to a *bis*-His 6cLS configuration in equilibrium with variable proportions of the native and 5cHS forms. These conformational changes can be modulated and eventually suppressed by controlling the interfacial electric field, which in turn depends on the electrode material and applied potential, on the thickness and functional groups of the SAMs, and on the pH and ionic strength of the solution.[9,16,17] Interestingly, the interaction of Cyt-c with the biologically relevant lipid cardiolipin (CL), both in solution[69] and upon adsorption of the Cyt-c/CL complex on SAM-coated electrodes, leads to similar conformational changes.[64] The alternative 5cHS conformation presents enhanced peroxidase and nitrite reductase activity.[64,66,67,69] The magnitude of the electric field operating at the SAM/protein interface was assessed through SEIRA measurements of the vibrational Stark effect experienced by nitrile reporters incorporated as head groups of the SAMs[70] and into the protein,[60] affording values comparable to those found at biological membranes.

Even under conditions that do not lead to conformational changes, the local electric fields play a crucial role in modulating the dynamics of Cyt-c in the electrostatic complexes, which in turn determines the electronic coupling, as verified by time-resolved SERR[33,47,48,54] and SEIRA[58,71] spectroelectrochemical experiments (TR-SERR and TR-SEIRA, respectively), as well as by electrochemically controlled plasmonic detection.[72] TR-SERR experiments also show that relatively weak electrostatic SAM/Cyt-c interactions that do not induce ligand exchange produce subtle deformations of the flexible Ω-loops that affect the H-bonding network and, more specifically, disrupt the Met80-Tyr67 H-bond.[59] The effect of this electrostatic perturbation, which implicates the same binding domain involved in interactions of Cyt-c with partner biomolecules, is a twofold decrease of the reorganization energy that facilitates ET. Thus, electrostatic interactions of Cyt-c crucially determine ET parameters and transitions to alternative conformations able to perform alternative functions. To shed more light on this topic, Oviedo-Rouco et al.[31,63] studied the heterogeneous ET reactions and conformational transitions of different Cyt-c variants adsorbed on SAM-coated electrodes by TR-SERR spectroelectrochemistry. The variants include the wild-type protein, the mutants Y67F and E66Q, and the WT protein nitrated at the Tyr74 residue (NO_2-Cyt-c). All of these proteins have a conserved Met/His axial coordination and largely superimposable structures, but differ in the flexibility of some specific regions (Figure 2B), mainly at the level of the Ω-loops 20−35, 40−57, and 70−85. Interestingly, the reduction potentials ($E^{o\prime}$) show a clear correlation with the root-mean-square fluctuations (RMSF) of the loop 40−57 (Figure 3A) and weaker dependencies with other structural elements (not shown).[31]

To assess whether these differences in protein flexibility also affect the conformational transitions, the pK_a of the so-called alkaline transition was determined for the same set of Cyt-c variants. This transition consists of the pH-induced replacement of the Met80 axial ligand by either Lys73 or Lys79 to yield Lys/His axial coordination.[25,63] The pK_a value of the transition is 9.4 for WT Cyt-c, and it shifts downwards and upwards for the other variants. As shown in Figure 3A, pK_a values tend to increase with the RMSF of the loop 70−85, but show no correlation with the flexibilities of the other two loops. Thus, the thermodynamic parameters that characterize the ET function and the transition to alternative conformations ($E^{o\prime}$ and pK_a, respectively) are modulated by the conformational flexibility of the protein, but each magnitude is fine-tuned by the flexibility of different structural elements.

Consistent with the results presented in the previous section, the ET activation energies of the four Cyt-c variants are higher

https://dx.doi.org/10.1021/acsomega.0c05746
ACS Omega 2021, 6, 3435−3446

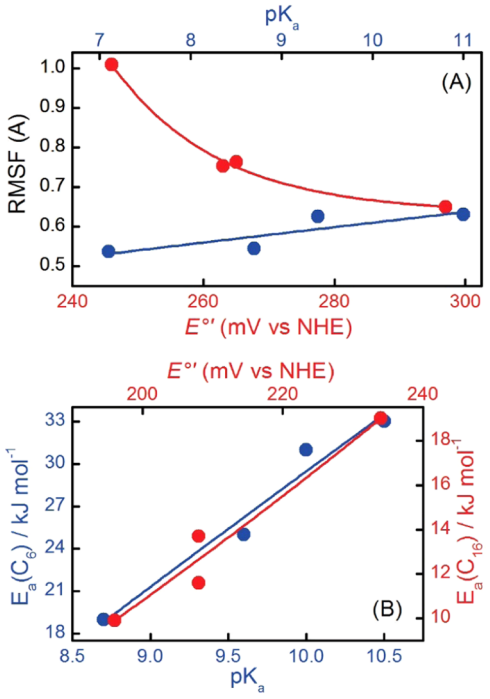

Figure 3. Correlations found for redox and conformational parameters of four Cyt-c variants: WT Cyt-c, Y67F, E66Q, and NO_2-Cyt-c. (A) Fluctuations of the Ω-loops 40−57 (red) and 70−85 (blue) as functions of the $E^{\circ\prime}$ and pK_a values, respectively. (B) ET activation energies measured at thin (blue) and thick (red) SAMs plotted as functions of the pK_a and $E^{\circ\prime}$ values, respectively. The lines are included to guide the eye. Adapted with permission from ref 31. Copyright 2020, Elsevier.

when measured at thin SAMs, i.e., in the friction-controlled regime (E_a(FC)), than at thick SAMs, i.e., in the nonadiabatic regime (E_a(NA)). Moreover, E_a(FC) increases with the pK_a′s of the alkaline transitions, while E_a(NA) shows an inverse dependency with $E^{\circ\prime}$ (Figure 3B). These cross-correlations suggest that E_a(FC) and pK_a are largely determined by the flexibility of the loop 70−85 while E_a(NA) and $E^{\circ\prime}$ are mostly influenced by the flexibility of the loop 40−57. As previously shown, the loop 70−85 contains most of the residues that constitute the binding site of Cyt-c to the SAMs (and to natural partners)[48] and, therefore, its flexibility is expected to modulate E_a(FC) through κ and E_s (eq 6). Moreover, this loop contains the Lys residues involved in the alkaline transitions and, therefore, its flexibility is expected to affect pK_a. On the other hand, the decrease of $E^{\circ\prime}$ values with increasing flexibility of the loop 40−57 is consistent with a higher accessibility of water molecules to the redox center, which is known to downshift $E^{\circ\prime}$ due to preferential stabilization of the Fe^{3+} form.[25] The parallel decrease of E_a (NA) is more difficult to rationalize as discrimination of inner-sphere (λ_{in}) and outer-sphere (λ_{out}) contributions is not trivial, but it has been argued that most likely it is related to a decrease of λ_{out} with increasing loop flexibility, rather than to variations of λ_{in}.[31]

One should note that in all of these studies of immobilized proteins, the measured quantities represent an average of all electroactive orientations. In the case of electrostatically adsorbed Cyt-c, this distribution of orientations is rather narrow as shown by MD simulations, SEIRA, and SERR experiments.[33,36,47,48,54,58,65]

In summary, TR-SERR spectroelectrochemical experiments demonstrate that for Cyt-c at interfaces of relatively low local electric fields the flexibility of the Ω-loops critically modulates the redox parameters of the native Cyt-c conformation and the transition to alternative conformations with a different functionality. These results are consistent with solution experiments showing that the pathogenic mutations G41S, Y48H, and A51V found in humans, and other modifications at the level of the loop 40−57, result in enhanced flexibility of both Ω-loops compared to the WT protein, which leads to higher peroxidase activity due to partial detachment of the axial ligand Met80, and lower pK_a and $E^{\circ\prime}$ values.[73−78]

Respiratory Complex IV. This integral membrane protein complex, also termed cytochrome *c* oxidase (CcO), is the terminal enzyme in aerobic respiration. It contains a Cu_A center that accepts electrons from Cyt-c, which are subsequently transferred to a heme *a* and from there to the catalytic binuclear heme a_3-Cu_B site where O_2 is reduced to H_2O. The process is coupled to proton translocation across the membrane. Steininger et al.[79] used TR-SEIRA to investigate the conformational changes of *R. sphaeroides* CcO occurring in the ms timescale during the enzymatic turnover, i.e., in the presence of O_2, and compared these results with previous studies under anaerobic conditions.[80] For these experiments, the enzyme containing an engineered His-tag was bound to a nitrile triacetic acid (NTA)-modified electrode followed by reconstitution into a lipid bilayer (Figure 4), as previously described.[81,82]

The His-tag was introduced into subunit II of the enzyme, which contains the Cu_A electron entry site, to allow for functional stepwise heterogeneous electron transfer from and to the electrode.

The immobilized enzyme was first electrochemically fully reduced at −800 mV. Thereafter, the potential was switched to the open-circuit value and the enzyme was allowed to perform enzymatic reoxidation in the presence of molecular oxygen. TR-SEIRA spectra were acquired using the step-scan mode, triggered by periodic potential pulses from −800 mV to the open-circuit potential. Changes of the protein secondary structure associated with the enzymatic turnover were assessed by phase sensitive detection of the amide I region (Figure 4). This analysis indicates a high flexibility of the secondary structure including the helices surrounding the catalytic center, which is higher for β-sheet elements compared to α-helices both under aerobic and anaerobic conditions. Conformational changes are faster in the case of reoxidation by oxygen compared to electrochemical reoxidation and reflect the full turnover of CcO.[79]

Following a different strategy, Sezer et al.[83] adsorbed detergent solubilized CcO from *R. sphaeroides* on Ag electrodes coated with NH_2-terminated SAMs that are meant to mimic the electrostatic binding of the enzyme to its electron donor Cyt-c. The integrity and electrochemical reduction of the enzyme was monitored by SERR. As in a previous work,[84] reduction of both hemes was monitored from the downshift of the ν_4 vibrational band, while the redox state of the heme a_3 was selectively assessed from the position and intensity of the isolated bands that arise from the vibrations of the formyl group. Under anaerobic conditions both hemes could be successfully reduced at potentials very close to those measured in solution, thus indicating the integrity of the centers. However, a significant population of solely heme *a* was found to undergo a conformational change in the adsorbed state that implies the loss of one His ligand, as revealed by SERR, and a concomitant

https://dx.doi.org/10.1021/acsomega.0c05746
ACS Omega 2021, 6, 3435−3446

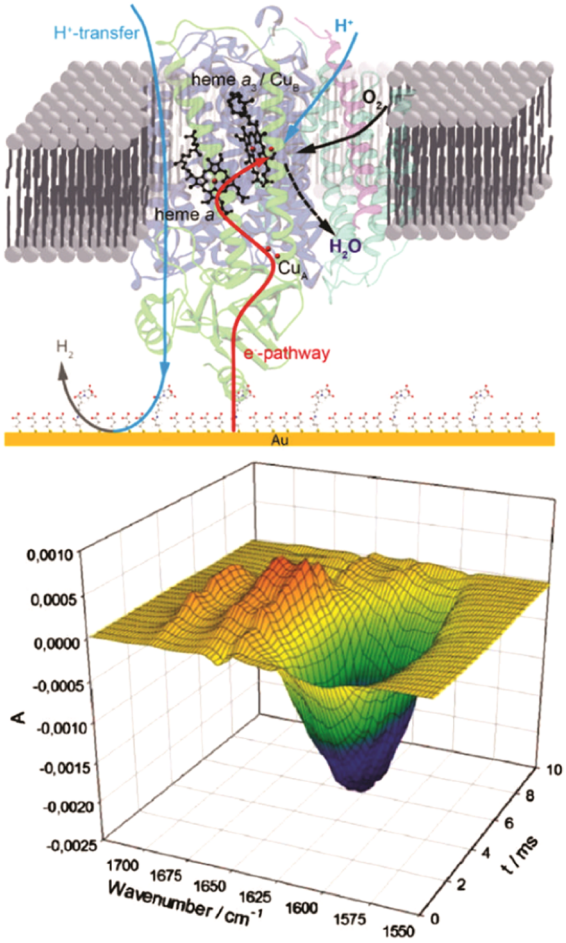

Figure 4. Top: Schematic representation of CcO immobilized via an engineered His-tag on a Ni−NTA-coated Au electrode and reconstituted into a lipid bilayer. Bottom: TR-SEIRA spectra of the amide I band recorded under aerobic conditions after a change of potentials from −0.8 V to the open-circuit potential. Adapted with permission from ref 70. Copyright 2016, Elsevier.

downshift of the reduction potential.[83] Using the same methodology, in combination with H_2O/D_2O experiments and QM−MM calculations, the authors were able to identify the resonant enhanced CH_2 twisting modes of the propionates of the individual hemes *a* and a_3, and their responses to the protonation state.[85] These studies reveal that at least three of the four heme propionates are protonated in the fully reduced enzyme, whereas for an intermediate redox state with the reduced heme *a* and oxidized heme a_3 only one heme a_3 propionate is protonated, thus supporting the involvement of this group in the proton pathway.[85] The PMIRRAS technique was also applied to monitor the adsorption of CcO on SAM-coated electrodes and to assess the integrity and orientation of the immobilized enzyme.[86]

A few other terminal O_2-reductases, such as the aa_3 quinol oxidase from *Acidianus ambivalens*,[87] the cbb_3 enzyme from *Bradyrhizobium japonicum*,[88] and the bo_3 ubiquinol oxidase from *Escherichia coli*[89] have also been investigated using SERR and SEIRA spectroelectrochemical methodologies.

Respiratory Complex I (CpI). CpI is a very large membrane enzyme catalyzing the first step of electron transport chains. It oxidizes NADH transferring electrons to membrane soluble ubiquinone, for which it is endowed with an internal chain of several redox groups including FMN and iron−sulfur clusters. The ET steps in the CpI drive proton translocation across the membrane. Gutiérrez-Sanz et al. used SEIRA to investigate the CpI from *R. marinus* in a biomimetic construct.[90] For this purpose CpI was incorporated into two types of unilamellar liposomes and the resulting proteoliposomes were deposited onto the Au-coated ATR crystal functionalized with a SAM of 4-aminothiophenol (Figure 5).

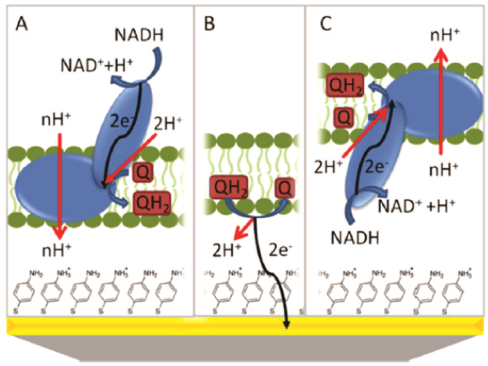

Figure 5. Schematic representation of the biomimetic construct of a CpI-lipid bilayer system adsorbed on a Au-coated ATR crystal functionalized with 4-aminothiophenol. Proton translocation leads to either acidification (A) or alkalinization (C) of the SAM surface, depending on CpI orientation. Electrochemical quinine reoxidation leads to acidification in both cases (B). Reproduced from ref 81. Copyright 2018, American Chemical Society.

Changes of the amide I/amide II band intensity ratio reveal conformational changes during catalysis, which may involve movements of transmembrane helices or other secondary structural elements. Moreover, the 4-aminothiophenol SAM is shown to behave as a SEIRA reporter of pH that responds to the local changes that result from the proton translocation activity of CpI (Figure 5). Santos Seica et al.[91] moved one step forward in monitoring conformational movements during the CpI turnover. To that end the authors introduced a small and highly flexible nitrile infrared label that allows to monitor intramolecular movements of CpI segments by SEIRA. Specifically, they labeled two residues belonging to the amphipathic helix across the membrane arm of CpI and anchored the protein to the Au-coated ATR crystal using the His-tag/Ni−NTA technique. SEIRA experiments show that the labeled residues move to a more hydrophobic environment upon NADH reduction of the enzyme, likely as a response to the reorganization of the antiporter-like subunits in the membrane arm.

Hydrogenases. [NiFe]-hydrogenases are a family of enzymes that contain a [NiFe] bimetallic active site in a large subunit where H_2 can be oxidized to H^+ and vice versa. A smaller ET subunit contains a chain of iron−sulfur clusters. In addition to terminal and bridging cysteine ligands, the [NiFe] center contains CN^- and CO coordinated to the iron. These unusual ligands are strongly IR-active and represent sensitive markers of the electronic state of the center, which has driven a large number of IR-based spectroscopic and spectroelectrochemical studies.[92,93] Spectroelectrochemical studies of electrode-confined hydrogenases are motivated both for structural and mechanistic fundamental aspects as well as for the technological interest of H_2 splitting as an energy source. For example, Zebger and co-workers[94−99] performed SEIRA studies of a variety of

https://dx.doi.org/10.1021/acsomega.0c05746
ACS Omega 2021, 6, 3435−3446

hydrogenases from different organisms immobilized on Au-coated ATR crystals using various immobilization procedures. This includes the attachment to a Ni−NTA-modified Au surface of the *Ralstonia eutropha* enzyme containing a C-terminus His-tag,[94] the electrostatic adsorption to SAMs of amino-terminated mercaptans of the enzymes from *Desulfovibrio vulgaris* [95−97] and *R. eutropha*,[98] as well as electrostatic adsorption of the *R. eutropha* enzyme to films of aromatic amines obtained by electrochemical reduction of diazonium salts.[99] The *D. vulgaris* enzyme has also been studied by SEIRA with its lipid tail inserted into a phospholipid bilayer supported on a 4-aminothiophenol SAM.[100] SEIRA characterization shows that the enzymes can be immobilized with preservation of the active site structure and with relatively uniform orientations that enable either direct or mediated ET and electrocatalytic H_2 oxidation. Voltammetric cycling is found to reversibly activate−inactivate the adsorbed enzyme, which could be related to specific intermediate-state redox couples and to a potential-induced enzyme reorientation.[95,96,98]

The alternative PFIRE approach introduced by Vincent and co-workers[19,101−103] consists of adsorbing the enzyme on a high surface area carbon electrode constructed from carbon black deposited onto a Si internal reflection element. The layer of enzyme-modified carbon particles is finally covered with carbon paper and a graphite connector. This approach allowed for the identification of catalytic intermediates in wild-type and single mutant hydrogenases, thus contributing to the elucidation of the catalytic mechanism.[102,103] For example, PFIRE experiments demonstrated that the so-called Ni−L state is an active catalytic intermediate of [NiFe] hydrogenases that for the *E. coli* enzyme can be generated reversibly in the dark at room temperature in a pH-dependent process.[19,101]

Multicopper Oxidases (MCO). This group of enzymes oxidize a variety of substrates by accepting electrons at a mononuclear copper center and transferring them to a trinuclear copper site where O_2 is reduced to H_2O. As oxygen reduction is the limiting step in fuel cells, substantial efforts are in progress to develop efficient biocathodes based on MCO such as laccases (LAC) and bilirubin oxidases (BOD). For example, Su et al.[104] studied adsorbed LAC on carbon nanotubes functionalized with naphthyl residues previously deposited onto a Au-coated ATR crystal for SEIRA characterization. Potential-dependent SEIRA spectra were analyzed using Fourier self-deconvolution and two-dimensional correlation spectroscopy to extract structural information from the amide I band. This analysis demonstrated that the adsorbed LAC retains the native structure in both oxidation states and, furthermore, reveals redox-linked conformational changes similar to the protein in solution. In agreement with these spectroscopic observations, the immobilized LAC shows excellent oxygen reduction activity.[104] Hitaishi et al.[20] used PMIRRAS to characterize the orientation and structural integrity of BOD in biocathodes constructed by electrostatic adsorption of the enzyme on SAM-coated Au electrodes at variable pH. They found out that the protein dipole moment and the charge in the vicinity of the electron entry Cu site drive the enzyme orientation. For weak electrostatic interactions, local pH variation affects the electron transfer rate as a result of protein mobility on the surface, while stronger electrostatic interactions destabilize the protein structure. Macedo et al.[22] developed a setup for in situ XAS and applied it to probe ET in BOD-based biocathodes during the oxygen reduction regime. The enzyme was directly adsorbed on carbon cloths oxidatively functionalized and covered with carbon nanoparticles to create a mesoporous structure. The electrochemical reduction of the BOD active site was monitored by following the attenuation of the XAS signal at 8997 eV attributed to Cu^{2+} and the rising of a signal at 8983 eV attributed to Cu^{+}. In the presence of molecular oxygen, BOD reduction requires an overpotential of about 150 mV compared to an inert atmosphere. These experiments provide evidence that the copper ions act as a tridimensional redox-active electronic bridge for the electron transfer reaction.

Blue Copper Proteins. These small soluble proteins function as electron shuttles using a mononuclear T1 copper center. Davis, Canters, and co-workers[21] introduced the concept of monitoring protein interfacial ET at optically transparent electrodes by means of redox-state-dependent fluorescence changes. The strategy consists of binding an organic fluorophore to the protein surface, to establish FRET between the dye and the redox site. The initial work was carried out with Cy5-labeled blue copper azurin adsorbed on alkyl-terminated SAMs using total internal reflection fluorescence microscopy (TIRF). This method, which was extended to other T1 blue copper and heme proteins,[105] demonstrated a high sensitivity that allowed for the spectroelectrochemical detection of a few hundred molecules in the earlier studies,[21,105,106] down to the direct and mediated single-molecule ET level in more recent developments by Akkilic et al.[107] and Pradhan et al.,[108] respectively. In the latter case, azurin was labeled with the dye ATTO647N and with biotin. The protein was immobilized on glasses previously functionalized with biotin and incubated with NeutrAvidin (Figure 6) and was subjected to a fixed applied potential using a ferricyanide redox mediator.

Analysis of the fluorescence time traces unveils significant fluctuations of the ET rates and reduction potentials that

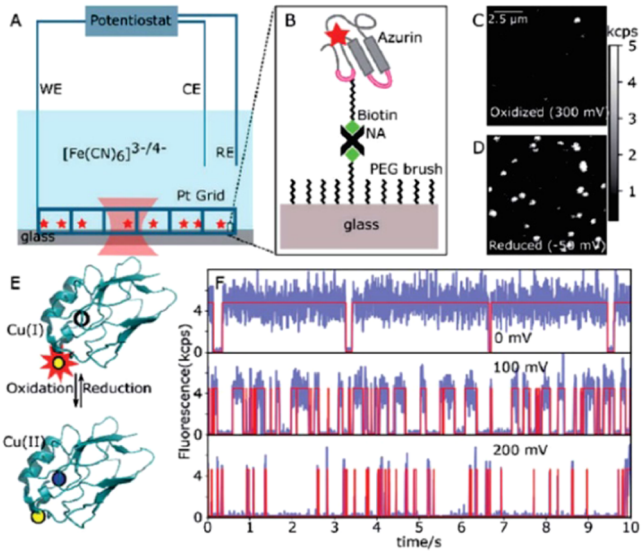

Figure 6. Single azurin (Azu) imaging and intensity traces at different potentials. (A) Spectroelectrochemical setup. (B) Schematic of the immobilization on PEG-passivated glass through NeutrAvidin−biotin binding. (C and D) Confocal images of the same area recorded at oxidizing and reducing potentials, respectively. (E) Azu structure containing reduced and oxidized Cu and the dye (yellow) in the fluorescence (top) and quenched (bottom) states, respectively. (F) Time traces of the same single Azu molecule recorded at different applied potentials. Reprinted with permission from ref 99. Copyright 2020, The Royal Society of Chemistry.

https://dx.doi.org/10.1021/acsomega.0c05746
ACS Omega 2021, 6, 3435−3446

indicate dynamical heterogeneity. The observed changes are ascribed mainly to variations in complex association constants and/or structural changes, as well as to changes in the reduction potential and electronic coupling to a lesser extent.[108]

Alcohol Dehydrogenase (ADH). NAD-dependent alcohol dehydrogenases (ADHs) catalyze the oxidation of alcohols to aldehydes and ketones with the concomitant reduction of NAD to NADH. Crespilho et al. developed setups for studying the electrocatalytic performance of enzymes adsorbed onto electrodes with either DMES[24] or in situ EPR[23] detection and applied them to immobilized ADH. The DEMS setup utilizes a flexible carbon fiber (FCF) working electrode, which facilitates the coupling of protein film voltammetry for monitoring NADH formation with mass spectrometry for detecting volatile intermediates and final products formed during enzymatic alcohol oxidation (Figure 7). The results confirm dissociation of

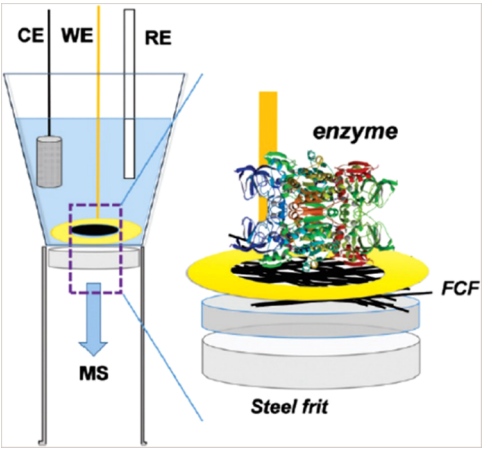

Figure 7. Schematic representation of the DEMS electrochemical cell. CE: counter-electrode, WE: working electrode, RE: reference electrode, and FCF: flexible carbon fiber array modified with ADH. The interface is constituted by a PTFE membrane over a steel frit. Reprinted with permission from ref 24. Copyright 2017, The Royal Society of Chemistry.

NADH as the rate-limiting step, thus favoring an ordered sequential Bi−Bi mechanism.[24] For EPR detection, the carbon fibers were functionalized with quinones, wherein the quantity of unpaired electron spins can be measured. The experiments show an increasing number of free unpaired electrons with increasing applied overpotentials and NADH oxidation, which suggests that the quinone groups on the carbon material electrocatalyze the oxidation of NADH to NAD^+.[23]

Other Redox Proteins and Enzymes. Moe et al.[109] used a combination of SEIRA and CV to study endonuclease III, a DNA glycosylase that removes oxidized pyrimidines from DNA, adsorbed on Au electrodes coated with SAMs of carboxyl-terminated alkanethiols and of normal and damaged DNA. The study shows that electrostatic interactions required for the redox activation of the enzyme may result in high electric fields that alter the structure and thermodynamic properties of the enzyme. It also indicates that the ET is modulated by subtle differences in the protein−DNA complex.

Kato et al.[110] used a combination of SEIRA and CV to determine the reduction potentials of the iron cofactors of *P. aeruginosa* NO-reductase. With the aid of CO as the vibrational probe, the researchers were able to show that the reduction of the heme b_3 initiates the enzymatic NO reduction.

Salewski et al.[111] studied *E. coli* Type II NADH:quinone oxidoreductase adsorbed on SAM-coated electrodes using SEIRA in combination with other spectroscopic and electrochemical methods. The study revealed two distinct substrate binding sites for NADH and the quinone and a bound semiprotonated quinol as a catalytic intermediate.

Todorovic et al. used SERR spectroelectrochemistry to characterize novel dye decolorizing peroxidases (DyP) adsorbed on SAM-coated electrodes. The studies reveal a well-preserved structure of the heme pocket for the adsorbed enzymes, albeit with altered spin populations with respect to the proteins in solution,[112] and allowed for the identification of a catalytic intermediate, most likely compound I.[113] Moreover, they found the immobilized DyP from *Pseudomonas putida* to outperform the broadly used HRP as the electrocatalytic biosensor for H_2O_2.[114]

Aiming to assess its potential for constructing biosensor devices, Silveira et al.[115] studied by SERR the periplasmic cytochrome PccH from *Geobacter sulfurreducens* adsorbed on SAMS with different functionalities. The structural and thermodynamic features of PccH are preserved upon attachment on mixed $-NH_2/-CH_3$ SAMs, while adsorption on single component $-OH$, $-NH_2$, and $-COOH$-functionalized SAMs leads to a distribution of native and non-native heme spin configurations.

Kielb et al.[116] used SERR for characterizing the redox properties of the hexameric tyrosine-coordinated heme protein (HTHP) from *Silicibacter pomeroyi*, which is known to exhibit peroxidase- and catalase-like activity. The experiments reveal two redox transitions at −0.17 and −0.54 V, which are attributed to different orientations of the protein on the SAM-coated Ag electrodes. Reduction is found to lead to partial loss of heme cofactors.

FUTURE OUTCOMES AND CHALLENGES

The immobilization of electron-transferring proteins and redox-active enzymes on electrode surfaces gives rise to significant interest because it enables electrochemical probing of their function in a simple way. It also sets the stage for the utilization of these macromolecules as building blocks for a variety of devices, including biosensors, biofuel cells, bioelectrocatalytic reactors, and bio-photovoltaic devices.

Protein immobilization, on the other hand, imposes conditions that may be quite distinct from solution in terms of local dielectric constants and electrostatic potentials, local ion concentrations, specific and unspecific interactions, and mobility. Therefore, immobilization strategies should be carefully designed to fulfill biomimicry or biocompatibility criteria, depending on the specific application. A meaningful in-depth assessment of the functional features of the immobilized proteins and enzymes is a significant challenge as it requires in situ or in operando investigation of the structure, orientation, conformational changes and dynamics, heterogeneous and intraprotein ET, enzymatic activity, catalytic cycle, and product generation. This can be achieved by hyphenating the electrochemical setup with a variety of spectroscopic methods, such as SERR, SEIRA, PFIRE, PMIRRAS, FRET, XAS, EPR, and DMES. In this perspective article, I have shown the value of these spectroelectrochemical techniques for elucidating complex aspects of ET and of redox-coupled reactions of a variety of immobilized proteins, including small heme and copper electron shuttling proteins, large respiratory complexes, hydrogenases, multicopper oxidases, alcohol dehydrogenases, endonucleases,

https://dx.doi.org/10.1021/acsomega.0c05746
ACS Omega 2021, 6, 3435−3446

NO-reductases, and dye decolorizing peroxidases, among others. The different methods provide largely complementary information, thus highlighting the advantages of multispectroscopic detection. In spite of that, most researchers base their studies on a single spectroelectrochemical technique, often due to restricted access to other methods and also due to inherent limitations of each method; not all spectroelectrochemical methods are suitable for all protein/electrode systems. For example, SERR detection is particularly useful for investigating the structure, electronic properties, and orientation of the active site of heme proteins, as attaining simultaneous resonance of the laser probe with the strong Soret absorption band of the heme and with the surface plasmons of Ag nanostructures is relatively simple. Although SERR spectroelectrochemistry is nowadays a well-established technology, there is still plenty of room for improvement in the reproducible nanofabrication of tunable SERR substrates, thus facilitating quantitative analysis and expansion to other redox proteins. IR-based methods, on the other hand, are sensitive to the protein orientation and secondary structure, as well as to conformational details, H-bonding, protonation of the peptide backbone, amino acid side chains, cofactors, and internal water molecules.[117] A drawback is their relatively low instrumental sensitivity, partially due to the low intensity of conventional light sources. The implementation of more intense light sources in routine setups, such as quantum cascade lasers, is a foreseeable development that may greatly expand the applicability of IR spectroelectrochemical techniques.[3] Other technical advancements that can be anticipated include the reproducible and cost-effective nanofabrication of SEIRA-active arrays, the expansion of DMES methods to the palette of available ionization methods, and improvements in the design of cells for magnetic and X-ray based spectroelectrochemical methods. Equally important is the development of advanced mathematical and computational tools for the reliable treatment of the large data sets that characterize stationary and time-resolved spectroelectrochemical experiments, particularly for the identification of unknown intermediate or transient species. Some of the most promising technologies in this respect include machine learning, neural networks, and wavelets.[4] The availability of highly sensitive spectroelectrochemical methods along with more powerful data processing tools will possibly guide the development of more comprehensive theoretical frameworks for the treatment of heterogeneous protein ET kinetics, will foster our fundamental understanding of redox proteins and enzymes and will contribute to the rational design of efficient protein-based technological devices.

AUTHOR INFORMATION

Corresponding Author

Daniel H. Murgida − *Departamento de Química Inorgánica, Analítica y Química-Física, Facultad de Ciencias Exactas y Naturales, Universidad de Buenos Aires, Buenos Aires 1428, Argentina; Instituto de Química Física de los Materiales, Medio Ambiente y Energía (INQUIMAE), CONICET-Universidad de Buenos Aires, Buenos Aires C1428EHA, Argentina;* orcid.org/0000-0001-5173-0183; Email: dhmurgida@qi.fcen.uba.ar

Complete contact information is available at: https://pubs.acs.org/10.1021/acsomega.0c05746

Notes

The author declares no competing financial interest.

ACKNOWLEDGMENTS

Financial support from ANPCyT (PICT2015−0133; PICT2018−4302) and UBACyT is gratefully acknowledged.

REFERENCES

(1) Liu, J.; Chakraborty, S.; Hosseinzadeh, P.; Yu, Y.; Tian, S.; Petrik, I.; Bhagi, A.; Lu, Y. Metalloproteins Containing Cytochrome, Iron−Sulfur, or Copper Redox Centers. *Chem. Rev.* **2014**, *114*, 4366−4469.

(2) Melin, F.; Hellwig, P. Redox Properties of the Membrane Proteins from the Respiratory Chain. *Chem. Rev.* **2020**, *120*, 10244−10297.

(3) Lozeman, J. J. A.; Führer, P.; Olthuis, W.; Odijk, M. Spectroelectrochemistry, the Future of Visualizing Electrode Processes by Hyphenating Electrochemistry with Spectroscopic Techniques. *Analyst* **2020**, *145*, 2482−2509.

(4) Garoz-Ruiz, J.; Perales-Rondon, J. V.; Heras, A.; Colina, A. Spectroelectrochemical Sensing: Current Trends and Challenges. *Electroanalysis* **2019**, *31*, 1254−1278.

(5) Yates, N. D. J.; Fascione, M. A.; Parkin, A. Methodologies for "Wiring" Redox Proteins/Enzymes to Electrode Surfaces. *Chem. - Eur. J.* **2018**, *24*, 12164−12182.

(6) Jenner, L. P.; Butt, J. N. Electrochemistry of Surface-Confined Enzymes: Inspiration, Insight and Opportunity for Sustainable Biotechnology. *Curr. Opin. Electrochem.* **2018**, *8*, 81−88.

(7) Ataka, K.; Stripp, S. T.; Heberle, J. Surface-Enhanced Infrared Absorption Spectroscopy (SEIRAS) to Probe Monolayers of Membrane Proteins. *Biochim. Biophys. Acta, Biomembr.* **2013**, *1828*, 2283−2293.

(8) Sezer, M.; Millo, D.; Weidinger, I. M.; Zebger, I.; Hildebrandt, P. Analyzing the Catalytic Processes of Immobilized Redox Enzymes by Vibrational Spectroscopies. *IUBMB Life* **2012**, *64*, 455−464.

(9) Murgida, D. H.; Hildebrandt, P. Electron-Transfer Processes of Cytochrome c at Interfaces. New Insights by Surface-Enhanced Resonance Raman Spectroscopy. *Acc. Chem. Res.* **2004**, *37*, 854−861.

(10) Léger, C.; Bertrand, P. Direct Electrochemistry of Redox Enzymes as a Tool for Mechanistic Studies. *Chem. Rev.* **2008**, *108*, 2379−2438.

(11) Evans, R. M.; Siritanaratkul, B.; Megarity, C. F.; Pandey, K.; Esterle, T. F.; Badiani, S.; Armstrong, F. A. The Value of Enzymes in Solar Fuels Research − Efficient Electrocatalysts through Evolution. *Chem. Soc. Rev.* **2019**, *48*, 2039−2052.

(12) Armstrong, F. A.; Evans, R. M.; Hexter, S. V.; Murphy, B. J.; Roessler, M. M.; Wulff, P. Guiding Principles of Hydrogenase Catalysis Instigated and Clarified by Protein Film Electrochemistry. *Acc. Chem. Res.* **2016**, *49*, 884−892.

(13) Ranieri, A.; Bortolotti, C. A.; Di Rocco, G.; Battistuzzi, G.; Sola, M.; Borsari, M. Electrocatalytic Properties of Immobilized Heme Proteins: Basic Principles and Applications. *ChemElectroChem* **2019**, *6*, 5172−5185.

(14) Bollella, P.; Katz, E. Enzyme-Based Biosensors: Tackling Electron Transfer Issues. *Sensors* **2020**, *20*, No. 3517.

(15) Kornienko, N.; Ly, K. H.; Robinson, W. E.; Heidary, N.; Zhang, J. Z.; Reisner, E. Advancing Techniques for Investigating the Enzyme−Electrode Interface. *Acc. Chem. Res.* **2019**, *52*, 1439−1448.

(16) Murgida, D. H.; Hildebrandt, P. Disentangling Interfacial Redox Processes of Proteins by SERR Spectroscopy. *Chem. Soc. Rev.* **2008**, *37*, 937−945.

(17) Ly, H. K.; Sezer, M.; Wisitruangsakul, N.; Feng, J.-J.; Kranich, A.; Millo, D.; Weidinger, I. M.; Zebger, I.; Murgida, D. H.; Hildebrandt, P. Surface-Enhanced Vibrational Spectroscopy for Probing Transient Interactions of Proteins with Biomimetic Interfaces: Electric Field Effects on Structure, Dynamics and Function of Cytochrome c. *FEBS J.* **2011**, *278*, 1382−1390.

(18) Ash, P. A.; Vincent, K. A. Spectroscopic Analysis of Immobilised Redox Enzymes under Direct Electrochemical Control. *Chem. Commun.* **2012**, *48*, 1400−1409.

(19) Hidalgo, R.; Ash, P. A.; Healy, A. J.; Vincent, K. A. Infrared Spectroscopy During Electrocatalytic Turnover Reveals the Ni-L Active

Site State During H2 Oxidation by a NiFe Hydrogenase. *Angew. Chem., Int. Ed.* **2015**, *54*, 7110−7113.
(20) Hitaishi, V. P.; Clément, R.; Quattrocchi, L.; Parent, P.; Duché, D.; Zuily, L.; Ilbert, M.; Lojou, E.; Mazurenko, I. Interplay between Orientation at Electrodes and Copper Activation of Thermus Thermophilus Laccase for O2 Reduction. *J. Am. Chem. Soc.* **2020**, *142*, 1394−1405.
(21) Davis, J. J.; Burgess, H.; Zauner, G.; Kuznetsova, S.; Salverda, J.; Aartsma, T.; Canters, G. W. Monitoring Interfacial Bioelectrochemistry Using a FRET Switch. *J. Phys. Chem. B* **2006**, *110*, 20649−20654.
(22) Macedo, L. J. A.; Hassan, A.; Sedenho, G. C.; Crespilho, F. N. Assessing Electron Transfer Reactions and Catalysis in Multicopper Oxidases with Operando X-Ray Absorption Spectroscopy. *Nat. Commun.* **2020**, *11*, No. 316.
(23) Ali, M. A.; Hassan, A.; Sedenho, G. C.; Gonçalves, R. V.; Cardoso, D. R.; Crespilho, F. N. Operando Electron Paramagnetic Resonance for Elucidating the Electron Transfer Mechanism of Coenzymes. *J. Phys. Chem. C* **2019**, *123*, 16058−16064.
(24) de Souza, J. C.; Silva, W. O.; Lima, F. H. B.; Crespilho, F. N. Enzyme Activity Evaluation by Differential Electrochemical Mass Spectrometry. *Chem. Commun.* **2017**, *53*, 8400−8402.
(25) Alvarez-Paggi, D.; Hannibal, L.; Castro, M. A.; Oviedo-Rouco, S.; Demicheli, V.; Tórtora, V.; Tomasina, F.; Radi, R.; Murgida, D. H. Multifunctional Cytochrome c: Learning New Tricks from an Old Dog. *Chem. Rev.* **2017**, *117*, 13382−13460.
(26) Zitare, U. A.; Szuster, J.; Scocozza, M. F.; Espinoza-Cara, A.; Leguto, A. J.; Morgada, M. N.; Vila, A. J.; Murgida, D. H. The Role of Molecular Crowding in Long-Range Metalloprotein Electron Transfer: Dissection into Site- and Scaffold-Specific Contributions. *Electrochim. Acta* **2019**, *294*, 117−125.
(27) Marcus, R. A.; Sutin, N. Electron Transfers in Chemistry and Biology. *Biochim. Biophys. Acta, Bioenerg.* **1985**, *811*, 265−322.
(28) De la Lande, A.; Cailliez, F.; Salahub, D. Electron Transfer Reactions in Enzymes: Seven Things That Might Break Down in Vanilla Marcus Theory and How to Fix Them If They Do. In *Simulating Enzyme Reactivity: Computational Methods in Enzyme Catalysis*; RSC Theoretical and Computational Chemistry Series; Royal Society of Chemistry, 2017; pp 89−149.
(29) Beratan, D. N.; Liu, C.; Migliore, A.; Polizzi, N. F.; Skourtis, S. S.; Zhang, P.; Zhang, Y. Charge Transfer in Dynamical Biosystems, or the Treachery of (Static) Images. *Acc. Chem. Res.* **2015**, *48*, 474−481.
(30) Blumberger, J. Recent Advances in the Theory and Molecular Simulation of Biological Electron Transfer Reactions. *Chem. Rev.* **2015**, *115*, 11191−11238.
(31) Oviedo-Rouco, S.; Perez-Bertoldi, J. M.; Spedalieri, C.; Castro, M. A.; Tomasina, F.; Tortora, V.; Radi, R.; Murgida, D. H. Electron Transfer and Conformational Transitions of Cytochrome c Are Modulated by the Same Dynamical Features. *Arch. Biochem. Biophys.* **2020**, *680*, No. 108243.
(32) Yue, H.; Khoshtariya, D.; Waldeck, D. H.; Grochol, J.; Hildebrandt, P.; Murgida, D. H. On the Electron Transfer Mechanism Between Cytochrome c and Metal Electrodes. Evidence for Dynamic Control at Short Distances. *J. Phys. Chem. B* **2006**, *110*, 19906−19913.
(33) Alvarez-Paggi, D.; Meister, W.; Kuhlmann, U.; Weidinger, I.; Tenger, K.; Zimányi, L.; Rákhely, G.; Hildebrandt, P.; Murgida, D. H. Disentangling Electron Tunneling and Protein Dynamics of Cytochrome c through a Rationally Designed Surface Mutation. *J. Phys. Chem. B* **2013**, *117*, 6061−6068.
(34) Monari, S.; Battistuzzi, G.; Bortolotti, C. A.; Yanagisawa, S.; Sato, K.; Li, C.; Salard, I.; Kostrz, D.; Borsari, M.; Ranieri, A.; Dennison, C.; Sola, M. Understanding the Mechanism of Short-Range Electron Transfer Using an Immobilized Cupredoxin. *J. Am. Chem. Soc.* **2012**, *134*, 11848−11851.
(35) Alvarez-Paggi, D.; Zitare, U.; Murgida, D. H. The Role of Protein Dynamics and Thermal Fluctuations in Regulating Cytochrome c/Cytochrome c Oxidase Electron Transfer. *Biochim. Biophys. Acta, Bioenerg.* **2014**, *1837*, 1196−1207.
(36) Capdevila, D. A.; Marmisollé, W. A.; Williams, F. J.; Murgida, D. H. Phosphate Mediated Adsorption and Electron Transfer of Cytochrome c. A Time-Resolved SERR Spectroelectrochemical Study. *Phys. Chem. Chem. Phys.* **2013**, *15*, 5386−5394.
(37) Khoshtariya, D. E.; Dolidze, T. D.; Shushanyan, M.; Davis, K. L.; Waldeck, D. H.; van Eldik, R. Fundamental Signatures of Short- and Long-Range Electron Transfer for the Blue Copper Protein Azurin at Au/SAM Junctions. *Proc. Natl. Acad. Sci. U.S.A.* **2010**, *107*, 2757−2762.
(38) Nahir, T. M.; Bowden, E. F. The Distribution of Standard Rate Constants for Electron Transfer between Thiol-Modified Gold Electrodes and Adsorbed Cytochrome c. *J. Electroanal. Chem.* **1996**, *410*, 9−13.
(39) El Kasmi, A.; Wallace, J. M.; Bowden, E. F.; Binet, S. M.; Linderman, R. J. Controlling Interfacial Electron-Transfer Kinetics of Cytochrome c with Mixed Self-Assembled Monolayers. *J. Am. Chem. Soc.* **1998**, *120*, 225−226.
(40) Avila, A.; Gregory, B. W.; Niki, K.; Cotton, T. M. An Electrochemical Approach to Investigate Gated Electron Transfer Using a Physiological Model System: Cytochrome c Immobilized on Carboxylic Acid-Terminated Alkanethiol Self-Assembled Monolayers on Gold Electrodes. *J. Phys. Chem. B* **2000**, *104*, 2759−2766.
(41) Jeuken, L. J. C. Conformational Reorganisation in Interfacial Protein Electron Transfer. *Biochim. Biophys. Acta, Bioenerg.* **2003**, *1604*, 67−76.
(42) Jeuken, L. J. C.; McEvoy, J. P.; Armstrong, F. A. Insights into Gated Electron-Transfer Kinetics at the Electrode−Protein Interface: A Square Wave Voltammetry Study of the Blue Copper Protein Azurin. *J. Phys. Chem. B* **2002**, *106*, 2304−2313.
(43) Chi, Q.; Zhang, J.; Andersen, J. E. T.; Ulstrup, J. Ordered Assembly and Controlled Electron Transfer of the Blue Copper Protein Azurin at Gold (111) Single-Crystal Substrates. *J. Phys. Chem. B* **2001**, *105*, 4669−4679.
(44) Fujita, K.; Nakamura, N.; Ohno, H.; Leigh, B. S.; Niki, K.; Gray, H. B.; Richards, J. H. Mimicking Protein−Protein Electron Transfer: Voltammetry of Pseudomonas Aeruginosa Azurin and the Thermus Thermophilus CuA Domain at ω-Derivatized Self-Assembled-Monolayer Gold Electrodes. *J. Am. Chem. Soc.* **2004**, *126*, 13954−13961.
(45) Wei, J.; Liu, H.; Khoshtariya, D. E.; Yamamoto, H.; Dick, A.; Waldeck, D. H. Electron-Transfer Dynamics of Cytochrome C: A Change in the Reaction Mechanism with Distance. *Angew. Chem., Int. Ed.* **2002**, *41*, 4700−4703.
(46) Khoshtariya, D. E.; Wei, J.; Liu, H.; Yue, H.; Waldeck, D. H. Charge-Transfer Mechanism for Cytochrome c Adsorbed on Nanometer Thick Films. Distinguishing Frictional Control from Conformational Gating. *J. Am. Chem. Soc.* **2003**, *125*, 7704−7714.
(47) Kranich, A.; Ly, H. K.; Hildebrandt, P.; Murgida, D. H. Direct Observation of the Gating Step in Protein Electron Transfer: Electric-Field-Controlled Protein Dynamics. *J. Am. Chem. Soc.* **2008**, *130*, 9844−9848.
(48) Alvarez-Paggi, D.; Martín, D. F.; Debiase, P. M.; Hildebrandt, P.; Martí, M. A.; Murgida, D. H. Molecular Basis of Coupled Protein and Electron Transfer Dynamics of Cytochrome c in Biomimetic Complexes. *J. Am. Chem. Soc.* **2010**, *132*, 5769−5778.
(49) Georg, S.; Kabuss, J.; Weidinger, I. M.; Murgida, D. H.; Hildebrandt, P.; Knorr, A.; Richter, M. Distance-Dependent Electron Transfer Rate of Immobilized Redox Proteins: A Statistical Physics Approach. *Phys. Rev. E* **2010**, *81*, No. 046101.
(50) Zitare, U. A.; Szuster, J.; Santalla, M. C.; Morgada, M. N.; Vila, A. J.; Murgida, D. H. Dynamical Effects in Metalloprotein Heterogeneous Electron Transfer. *Electrochim. Acta* **2020**, *342*, No. 136095.
(51) Zitare, U. A.; Szuster, J.; Santalla, M. C.; Llases, M. E.; Morgada, M. N.; Vila, A. J.; Murgida, D. H. Fine Tuning of Functional Features of the CuA Site by Loop-Directed Mutagenesis. *Inorg. Chem.* **2019**, *58*, 2149−2157.
(52) Matyushov, D. V. Dynamical Effects in Protein Electrochemistry. *J. Phys. Chem. B* **2019**, *123*, 7290−7301.
(53) Seyedi, S. S.; Waskasi, M. M.; Matyushov, D. V. Theory and Electrochemistry of Cytochrome c. *J. Phys. Chem. B* **2017**, *121*, 4958−4967.
(54) Ly, H. K.; Marti, M. A.; Martin, D. F.; Alvarez-Paggi, D.; Meister, W.; Kranich, A.; Weidinger, I. M.; Hildebrandt, P.; Murgida, D. H.

https://dx.doi.org/10.1021/acsomega.0c05746
ACS Omega 2021, 6, 3435−3446

Thermal Fluctuations Determine the Electron-Transfer Rates of Cytochrome c in Electrostatic and Covalent Complexes. *ChemPhysChem* **2010**, *11*, 1225−1235.
(55) Santucci, R.; Sinibaldi, F.; Cozza, P.; Polticelli, F.; Fiorucci, L. Cytochrome c: An Extreme Multifunctional Protein with a Key Role in Cell Fate. *Int. J. Biol. Macromol.* **2019**, *136*, 1237−1246.
(56) Hildebrandt, P.; Stockburger, M. Cytochrome c at Charged Interfaces. 1. Conformational and Redox Equilibria at the Electrode/Electrolyte Interface Probed by Surface-Enhanced Resonance Raman Spectroscopy. *Biochemistry* **1989**, *28*, 6710−6721.
(57) Buhrke, D.; Hildebrandt, P. Probing Structure and Reaction Dynamics of Proteins Using Time-Resolved Resonance Raman Spectroscopy. *Chem. Rev.* **2020**, *120*, 3577−3630.
(58) Wisitruangsakul, N.; Zebger, I.; Ly, K. H.; Murgida, D. H.; Ekgasit, S.; Hildebrandt, P. Redox-Linked Protein Dynamics of Cytochrome c Probed by Time-Resolved Surface Enhanced Infrared Absorption Spectroscopy. *Phys. Chem. Chem. Phys.* **2008**, *10*, 5276−5286.
(59) Alvarez-Paggi, D.; Castro, M. A.; Tórtora, V.; Castro, L.; Radi, R.; Murgida, D. H. Electrostatically Driven Second-Sphere Ligand Switch between High and Low Reorganization Energy Forms of Native Cytochrome c. *J. Am. Chem. Soc.* **2013**, *135*, 4389−4397.
(60) Biava, H.; Schreiber, T.; Katz, S.; Völler, J.-S.; Stolarski, M.; Schulz, C.; Michael, N.; Budisa, N.; Kozuch, J.; Utesch, T.; Hildebrandt, P. Long-Range Modulations of Electric Fields in Proteins. *J. Phys. Chem. B* **2018**, *122*, 8330−8342.
(61) Talaga, D.; Bremner, A.; Buffeteau, T.; Vallée, R. A. L.; Lecomte, S.; Bonhommeau, S. Total Internal Reflection Tip-Enhanced Raman Spectroscopy of Cytochrome c. *J. Phys. Chem. Lett.* **2020**, *11*, 3835−3840.
(62) Millo, D.; Bonifacio, A.; Ranieri, A.; Borsari, M.; Gooijer, C.; van der Zwan, G. PH-Induced Changes in Adsorbed Cytochrome c. Voltammetric and Surface-Enhanced Resonance Raman Characterization Performed Simultaneously at Chemically Modified Silver Electrodes. *Langmuir* **2007**, *23*, 9898−9904.
(63) Oviedo-Rouco, S.; Castro, M. A.; Alvarez-Paggi, D.; Spedalieri, C.; Tortora, V.; Tomasina, F.; Radi, R.; Murgida, D. H. The Alkaline Transition of Cytochrome c Revisited: Effects of Electrostatic Interactions and Tyrosine Nitration on the Reaction Dynamics. *Arch. Biochem. Biophys.* **2019**, *665*, 96−106.
(64) Ranieri, A.; Millo, D.; Di Rocco, G.; Battistuzzi, G.; Bortolotti, C. A.; Borsari, M.; Sola, M. Immobilized Cytochrome c Bound to Cardiolipin Exhibits Peculiar Oxidation State-Dependent Axial Heme Ligation and Catalytically Reduces Dioxygen. *J. Biol. Inorg. Chem.* **2015**, *20*, 531−540.
(65) Ataka, K.; Heberle, J. Functional Vibrational Spectroscopy of a Cytochrome c Monolayer: SEIDAS Probes the Interaction with Different Surface-Modified Electrodes. *J. Am. Chem. Soc.* **2004**, *126*, 9445−9457.
(66) Lancellotti, L.; Borsari, M.; Bonifacio, A.; Bortolotti, C. A.; Di Rocco, G.; Casalini, S.; Ranieri, A.; Battistuzzi, G.; Sola, M. Adsorbing Surface Strongly Influences the Pseudoperoxidase and Nitrite Reductase Activity of Electrode-Bound Yeast Cytochrome c. The Effect of Hydrophobic Immobilization. *Bioelectrochemistry* **2020**, *136*, No. 107628.
(67) Capdevila, D. A.; Marmisollé, W. A.; Tomasina, F.; Demicheli, V.; Portela, M.; Radi, R.; Murgida, D. H. Specific Methionine Oxidation of Cytochrome c in Complexes with Zwitterionic Lipids by Hydrogen Peroxide: Potential Implications for Apoptosis. *Chem. Sci.* **2015**, *6*, 705−713.
(68) Feng, J.-J.; Murgida, D. H.; Kuhlmann, U.; Utesch, T.; Mroginski, M. A.; Hildebrandt, P.; Weidinger, I. M. Gated Electron Transfer of Yeast Iso-1 Cytochrome c on Self-Assembled Monolayer-Coated Electrodes. *J. Phys. Chem. B* **2008**, *112*, 15202−15211.
(69) Capdevila, D. A.; Oviedo, R.; Tomasina, F.; Tortora, V.; Demicheli, V.; Radi, R.; Murgida, D. H. Active Site Structure and Peroxidase Activity of Oxidatively Modified Cytochrome c Species in Complexes with Cardiolipin. *Biochemistry* **2015**, *54*, 7491−7504.
(70) Staffa, J. K.; Lorenz, L.; Stolarski, M.; Murgida, D. H.; Zebger, I.; Utesch, T.; Kozuch, J.; Hildebrandt, P. Determination of the Local Electric Field at Au/SAM Interfaces Using the Vibrational Stark Effect. *J. Phys. Chem. C* **2017**, *121*, 22274−22285.
(71) Jin, B.; Wang, G.-X.; Millo, D.; Hildebrandt, P.; Xia, X.-H. Electric-Field Control of the PH-Dependent Redox Process of Cytochrome c Immobilized on a Gold Electrode. *J. Phys. Chem. C* **2012**, *116*, 13038−13044.
(72) Wang, Y.; Wang, H.; Chen, Y.; Wang, Y.; Chen, H.-Y.; Shan, X.; Tao, N. Fast Electrochemical and Plasmonic Detection Reveals Multitime Scale Conformational Gating of Electron Transfer in Cytochrome c. *J. Am. Chem. Soc.* **2017**, *139*, 7244−7249.
(73) Deacon, O. M.; Karsisiotis, A. I.; Moreno-Chicano, T.; Hough, M. A.; Macdonald, C.; Blumenschein, T. M. A.; Wilson, M. T.; Moore, G. R.; Worrall, J. A. R. Heightened Dynamics of the Oxidized Y48H Variant of Human Cytochrome c Increases Its Peroxidatic Activity. *Biochemistry* **2017**, *56*, 6111−6124.
(74) Lei, H.; Bowler, B. E. Naturally Occurring A51V Variant of Human Cytochrome c Destabilizes the Native State and Enhances Peroxidase Activity. *J. Phys. Chem. B* **2019**, *123*, 8939−8953.
(75) Deacon, O. M.; White, R. W.; Moore, G. R.; Wilson, M. T.; Worrall, J. A. R. Comparison of the Structural Dynamic and Mitochondrial Electron-Transfer Properties of the Proapoptotic Human Cytochrome c Variants, G41S, Y48H and A51V. *J. Inorg. Biochem.* **2020**, *203*, No. 110924.
(76) Karsisiotis, A. I.; Deacon, O. M.; Wilson, M. T.; MacDonald, C.; Blumenschein, T. M. A.; Moore, G. R.; Worrall, J. A. R. Increased Dynamics in the 40-57 Ω-Loop of the G41S Variant of Human Cytochrome c Promote Its pro-Apoptotic Conformation. *Sci. Rep.* **2016**, *6*, No. 30447.
(77) Moreno-Beltrán, B.; Guerra-Castellano, A.; Díaz-Quintana, A.; Conte, R. D.; García-Mauriño, S. M.; Díaz-Moreno, S.; González-Arzola, K.; Santos-Ocaña, C.; Velázquez-Campoy, A.; Rosa, M. A. D.; la Turano, P.; Díaz-Moreno, I. Structural Basis of Mitochondrial Dysfunction in Response to Cytochrome c Phosphorylation at Tyrosine 48. *Proc. Natl. Acad. Sci. U.S.A.* **2017**, *114*, E3041−E3050.
(78) García-Heredia, J. M.; Díaz-Quintana, A.; Salzano, M.; Orzáez, M.; Pérez-Payá, E.; Teixeira, M.; De la Rosa, M. A.; Díaz-Moreno, I. Tyrosine Phosphorylation Turns Alkaline Transition into a Biologically Relevant Process and Makes Human Cytochrome c Behave as an Anti-Apoptotic Switch. *J. Biol. Inorg. Chem.* **2011**, *16*, 1155−1168.
(79) Steininger, C.; Reiner-Rozman, C.; Schwaighofer, A.; Knoll, W.; Naumann, R. L. C. Kinetics of Cytochrome c Oxidase from *R. sphaeroides* Initiated by Direct Electron Transfer Followed by Tr-SEIRAS. *Bioelectrochemistry* **2016**, *112*, 1−8.
(80) Schwaighofer, A.; Ferguson-Miller, S.; Naumann, R. L. C.; Knoll, W.; Nowak, C. Phase-Sensitive Detection in Modulation Excitation Spectroscopy Applied to Potential Induced Electron Transfer in Cytochrome c Oxidase. *Appl. Spectrosc.* **2014**, *68*, 5−13.
(81) Giess, F.; Friedrich, M. G.; Heberle, J.; Naumann, R. L.; Knoll, W. The Protein-Tethered Lipid Bilayer: A Novel Mimic of the Biological Membrane. *Biophys. J.* **2004**, *87*, 3213−3220.
(82) Friedrich, M. G.; Gieß, F.; Naumann, R.; Knoll, W.; Ataka, K.; Heberle, J.; Hrabakova, J.; Murgida, D. H.; Hildebrandt, P. Active Site Structure and Redox Processes of Cytochrome c Oxidase Immobilised in a Novel Biomimetic Lipid Membrane on an Electrode. *Chem. Commun.* **2004**, *10*, 2376−2377.
(83) Sezer, M.; Kielb, P.; Kuhlmann, U.; Mohrmann, H.; Schulz, C.; Heinrich, D.; Schlesinger, R.; Heberle, J.; Weidinger, I. M. Surface Enhanced Resonance Raman Spectroscopy Reveals Potential Induced Redox and Conformational Changes of Cytochrome c Oxidase on Electrodes. *J. Phys. Chem. B* **2015**, *119*, 9586−9591.
(84) Hrabakova, J.; Ataka, K.; Heberle, J.; Hildebrandt, P.; Murgida, D. H. Long Distance Electron Transfer in Cytochrome c Oxidase Immobilised on Electrodes. A Surface Enhanced Resonance Raman Spectroscopic Study. *Phys. Chem. Chem. Phys.* **2006**, *8*, 759−766.
(85) Sezer, M.; Woelke, A.-L.; Knapp, E. W.; Schlesinger, R.; Mroginski, M. A.; Weidinger, I. M. Redox Induced Protonation of Heme Propionates in Cytochrome c Oxidase: Insights from Surface

https://dx.doi.org/10.1021/acsomega.0c05746
ACS Omega 2021, 6, 3435−3446

Enhanced Resonance Raman Spectroscopy and QM/MM Calculations. *Biochim. Biophys. Acta, Bioenerg.* **2017**, *1858*, 103−108.
(86) Mondal, P. C.; Fontanesi, C. Electrochemistry of Metalloproteins Attached through Functional Self-Assembled Monolayers on Gold and Ferromagnetic Electrodes. *ChemPhysChem* **2018**, *19*, 60−66.
(87) Todorovic, S.; Pereira, M. M.; Bandeiras, T. M.; Teixeira, M.; Hildebrandt, P.; Murgida, D. H. Midpoint Potentials of Hemes a and A3 in the Quinol Oxidase from *Acidianus ambivalens* Are Inverted. *J. Am. Chem. Soc.* **2005**, *127*, 13561−13566.
(88) Todorovic, S.; Verissimo, A.; Wisitruangsakul, N.; Zebger, I.; Hildebrandt, P.; Pereira, M. M.; Teixeira, M.; Murgida, D. H. SERR-Spectroelectrochemical Study of a cbb_3 Oxygen Reductase in a Biomimetic Construct. *J. Phys. Chem. B* **2008**, *112*, 16952−16959.
(89) Wiebalck, S.; Kozuch, J.; Forbrig, E.; Tzschucke, C. C.; Jeuken, L. J. C.; Hildebrandt, P. Monitoring the Transmembrane Proton Gradient Generated by Cytochrome Bo3 in Tethered Bilayer Lipid Membranes Using SEIRA Spectroscopy. *J. Phys. Chem. B* **2016**, *120*, 2249−2256.
(90) Gutiérrez-Sanz, O.; Forbrig, E.; Batista, A. P.; Pereira, M. M.; Salewski, J.; Mroginski, M. A.; Götz, R.; De Lacey, A. L.; Kozuch, J.; Zebger, I. Catalytic Activity and Proton Translocation of Reconstituted Respiratory Complex I Monitored by Surface-Enhanced Infrared Absorption Spectroscopy. *Langmuir* **2018**, *34*, 5703−5711.
(91) Santos Seica, A. F. S.; Schimpf, J.; Friedrich, T.; Hellwig, P. Visualizing the Movement of the Amphipathic Helix in the Respiratory Complex I Using a Nitrile Infrared Probe and SEIRAS. *FEBS Lett.* **2020**, *594*, 491−496.
(92) Ash, P. A.; Hidalgo, R.; Vincent, K. A. Proton Transfer in the Catalytic Cycle of [NiFe] Hydrogenases: Insight from Vibrational Spectroscopy. *ACS Catal.* **2017**, *7*, 2471−2485.
(93) Ash, P. A.; Kendall-Price, S. E. T.; Vincent, K. A. Unifying Activity, Structure, and Spectroscopy of [NiFe] Hydrogenases: Combining Techniques To Clarify Mechanistic Understanding. *Acc. Chem. Res.* **2019**, *52*, 3120−3131.
(94) Wisitruangsakul, N.; Lenz, O.; Ludwig, M.; Friedrich, B.; Lendzian, F.; Hildebrandt, P.; Zebger, I. Monitoring Catalysis of the Membrane-Bound Hydrogenase from *Ralstonia eutropha* H16 by Surface-Enhanced IR Absorption Spectroscopy. *Angew. Chem., Int. Ed.* **2009**, *48*, 611−613.
(95) Millo, D.; Pandelia, M.-E.; Utesch, T.; Wisitruangsakul, N.; Mroginski, M. A.; Lubitz, W.; Hildebrandt, P.; Zebger, I. Spectroelectrochemical Study of the [NiFe] Hydrogenase from *Desulfovibrio vulgaris* Miyazaki F in Solution and Immobilized on Biocompatible Gold Surfaces. *J. Phys. Chem. B* **2009**, *113*, 15344−15351.
(96) Millo, D.; Hildebrandt, P.; Pandelia, M.-E.; Lubitz, W.; Zebger, I. SEIRA Spectroscopy of the Electrochemical Activation of an Immobilized [NiFe] Hydrogenase under Turnover and Non-Turnover Conditions. *Angew. Chem., Int. Ed.* **2011**, *50*, 2632−2634.
(97) Utesch, T.; Millo, D.; Castro, M. A.; Hildebrandt, P.; Zebger, I.; Mroginski, M. A. Effect of the Protonation Degree of a Self-Assembled Monolayer on the Immobilization Dynamics of a [NiFe] Hydrogenase. *Langmuir* **2013**, *29*, 673−682.
(98) Heidary, N.; Utesch, T.; Zerball, M.; Horch, M.; Millo, D.; Fritsch, J.; Lenz, O.; von Klitzing, R.; Hildebrandt, P.; Fischer, A.; Mroginski, M. A.; Zebger, I. Orientation-Controlled Electrocatalytic Efficiency of an Adsorbed Oxygen-Tolerant Hydrogenase. *PLoS One* **2015**, *10*, No. e0143101.
(99) Harris, T. G. A. A.; Heidary, N.; Kozuch, J.; Frielingsdorf, S.; Lenz, O.; Mroginski, M.-A.; Hildebrandt, P.; Zebger, I.; Fischer, A. In Situ Spectroelectrochemical Studies into the Formation and Stability of Robust Diazonium-Derived Interfaces on Gold Electrodes for the Immobilization of an Oxygen-Tolerant Hydrogenase. *ACS Appl. Mater. Interfaces* **2018**, *10*, 23380−23391.
(100) Gutiérrez-Sanz, O.; Marques, M.; Pereira, I. A. C.; De Lacey, A. L.; Lubitz, W.; Rüdiger, O. Orientation and Function of a Membrane-Bound Enzyme Monitored by Electrochemical Surface-Enhanced Infrared Absorption Spectroscopy. *J. Phys. Chem. Lett.* **2013**, *4*, 2794−2798.
(101) Murphy, B. J.; Hidalgo, R.; Roessler, M. M.; Evans, R. M.; Ash, P. A.; Myers, W. K.; Vincent, K. A.; Armstrong, F. A. Discovery of Dark PH-Dependent H^+ Migration in a [NiFe]-Hydrogenase and Its Mechanistic Relevance: Mobilizing the Hydrido Ligand of the Ni-C Intermediate. *J. Am. Chem. Soc.* **2015**, *137*, 8484−8489.
(102) Ash, P. A.; Liu, J.; Coutard, N.; Heidary, N.; Horch, M.; Gudim, I.; Simler, T.; Zebger, I.; Lenz, O.; Vincent, K. A. Electrochemical and Infrared Spectroscopic Studies Provide Insight into Reactions of the NiFe Regulatory Hydrogenase from *Ralstonia eutropha* with O_2 and CO. *J. Phys. Chem. B* **2015**, *119*, 13807−13815.
(103) Evans, R. M.; Ash, P. A.; Beaton, S. E.; Brooke, E. J.; Vincent, K. A.; Carr, S. B.; Armstrong, F. A. Mechanistic Exploitation of a Self-Repairing, Blocked Proton Transfer Pathway in an O_2-Tolerant [NiFe]-Hydrogenase. *J. Am. Chem. Soc.* **2018**, *140*, 10208−10220.
(104) Su, Z.; Karaskiewicz, M.; Rogalski, J.; Bilewicz, R.; Lipkowski, J. Spectroelectrochemical Studies of Structural Changes during Reduction of Oxygen Catalyzed by Laccase Adsorbed on Modified Carbon Nanotubes. *J. Electroanal. Chem.* **2020**, No. 113820.
(105) Kuznetsova, S.; Zauner, G.; Schmauder, R.; Mayboroda, O. A.; Deelder, A. M.; Aartsma, T. J.; Canters, G. W. A Förster-Resonance-Energy Transfer-Based Method for Fluorescence Detection of the Protein Redox State. *Anal. Biochem.* **2006**, *350*, 52−60.
(106) Salverda, J. M.; Patil, A. V.; Mizzon, G.; Kuznetsova, S.; Zauner, G.; Akkilic, N.; Canters, G. W.; Davis, J. J.; Heering, H. A.; Aartsma, T. J. Fluorescent Cyclic Voltammetry of Immobilized Azurin: Direct Observation of Thermodynamic and Kinetic Heterogeneity. *Angew. Chem., Int. Ed.* **2010**, *49*, 5776−5779.
(107) Akkilic, N.; Kamran, M.; Stan, R.; Sanghamitra, N. J. M. Voltage-Controlled Fluorescence Switching of a Single Redox Protein. *Biosens. Bioelectron.* **2015**, *67*, 747−751.
(108) Pradhan, B.; Engelhard, C.; Mulken, S. V.; Miao, X.; Canters, G. W.; Orrit, M. Single Electron Transfer Events and Dynamical Heterogeneity in the Small Protein Azurin from Pseudomonas Aeruginosa. *Chem. Sci.* **2020**, *11*, 763−771.
(109) Moe, E.; Rollo, F.; Silveira, C. M.; Sezer, M.; Hildebrandt, P.; Todorovic, S. Spectroelectrochemical Insights into Structural and Redox Properties of Immobilized Endonuclease III and Its Catalytically Inactive Mutant. *Spectrochim. Acta, Part A* **2018**, *188*, 149−154.
(110) Kato, M.; Nakagawa, S.; Tosha, T.; Shiro, Y.; Masuda, Y.; Nakata, K.; Yagi, I. Surface-Enhanced Infrared Absorption Spectroscopy of Bacterial Nitric Oxide Reductase under Electrochemical Control Using a Vibrational Probe of Carbon Monoxide. *J. Phys. Chem. Lett.* **2018**, *9*, 5196−5200.
(111) Salewski, J.; Batista, A. P.; Sena, F. V.; Millo, D.; Zebger, I.; Pereira, M. M.; Hildebrandt, P. Substrate−Protein Interactions of Type II NADH:Quinone Oxidoreductase from Escherichia Coli. *Biochemistry* **2016**, *55*, 2722−2734.
(112) Sezer, M.; Santos, A.; Kielb, P.; Pinto, T.; Martins, L. O.; Todorovic, S. Distinct Structural and Redox Properties of the Heme Active Site in Bacterial Dye Decolorizing Peroxidase-Type Peroxidases from Two Subfamilies: Resonance Raman and Electrochemical Study. *Biochemistry* **2013**, *52*, 3074−3084.
(113) Todorovic, S.; Hildebrandt, P.; Martins, L. O. Surface Enhanced Resonance Raman Detection of a Catalytic Intermediate of DyP-Type Peroxidase. *Phys. Chem. Chem. Phys.* **2015**, *17*, 11954−11957.
(114) Barbosa, C.; Silveira, C. M.; Silva, D.; Brissos, V.; Hildebrandt, P.; Martins, L. O.; Todorovic, S. Immobilized Dye-Decolorizing Peroxidase (DyP) and Directed Evolution Variants for Hydrogen Peroxide Biosensing. *Biosens. Bioelectron.* **2020**, *153*, No. 112055.
(115) Silveira, C. M.; Castro, M. A.; Dantas, J. M.; Salgueiro, C.; Murgida, D. H.; Todorovic, S. Structure, Electrocatalysis and Dynamics of Immobilized Cytochrome PccH and Its Microperoxidase. *Phys. Chem. Chem. Phys.* **2017**, *19*, 8908−8918.
(116) Kielb, P.; Utesch, T.; Kozuch, J.; Jeoung, J.-H.; Dobbek, H.; Mroginski, M. A.; Hildebrandt, P.; Weidinger, I. Switchable Redox Chemistry of the Hexameric Tyrosine-Coordinated Heme Protein. *J. Phys. Chem. B* **2017**, *121*, 3955−3964.
(117) Lorenz-Fonfria, V. A. Infrared Difference Spectroscopy of Proteins: From Bands to Bonds. *Chem. Rev.* **2020**, *120*, 3466−3576.

https://dx.doi.org/10.1021/acsomega.0c05746
ACS Omega 2021, 6, 3435−3446